

# Photoluminescence Study of Carrier Localization and Recombination in Nearly Strain-Balanced Nonpolar InGaN/AlGaN Quantum Wells

Yang Cao, Brandon Dzuba, Brenden A. Magill, Alexander Senichev, Trang Nguyen, Rosa E. Diaz, Michael J. Manfra, Stephen McGill, Carlos Garcia, Giti A. Khodaparast, and Oana Malis\*


Temperature-dependent continuous-excitation and time-resolved photoluminescence are studied to probe carrier localization and recombination in nearly strain-balanced *m*-plane  $\text{In}_{0.09}\text{Ga}_{0.91}\text{N}/\text{Al}_{0.19}\text{Ga}_{0.81}\text{N}$  multi-quantum wells grown by plasma-assisted molecular-beam epitaxy. An average localization depth of 21 meV is estimated for the undoped sample. This depth is much smaller than the reported values in polar structures and *m*-plane InGaN quantum wells. As part of this study, temperature and magnetic field dependence of time-resolved photoluminescence is performed. At 2 K, an initial fast decay time of  $\approx 0.3$  ns is measured for both undoped and doped structures. The undoped sample also exhibits a slow decay component with a time scale of 2.2 ns. The existence of two relaxation paths in the undoped structure can be attributed to different localization centers. The fast relaxation decays are relatively insensitive to external magnetic fields, while the slower relaxation time constant decreases significantly with increasing magnetic fields. The fast decay time scale in the undoped sample is likely due to indium fluctuations in the quantum well. The slow decay time may be related to carrier localization in the barriers. The addition of doping leads to a single fast decay time likely due to stronger exciton localization in the InGaN quantum wells.

## 1. Introduction

The large bandgap range (0.7 to 6.2 eV), and large conduction band offsets of III-nitride semiconductors make applications of these materials in optoelectronic devices possible in a wide wavelength range from ultraviolet to far-infrared.<sup>[1–4]</sup> To date, polar *c*-plane III-nitride heterostructures have been most extensively studied. However, electric fields greater than  $10^5$  V cm<sup>-1</sup> are produced by large discontinuities of spontaneous and piezoelectric polarizations at hetero-interfaces in *c*-plane nitride quantum wells (QWs).<sup>[5–8]</sup> As a result, the electron and hole wave functions are separated leading to reduced internal quantum efficiency (IQE) and increased recombination lifetimes.<sup>[8]</sup> Moreover, the design of infrared intersubband devices is restricted by those electric fields.<sup>[9–12]</sup> To eliminate the deleterious effects of built-in electric fields, nonpolar *m*-plane heterostructures have been proposed. Nonpolar InGaN QWs have been chosen as candidates for

Y. Cao, B. Dzuba, A. Senichev, T. Nguyen, M. J. Manfra, O. Malis  
Department of Physics and Astronomy  
Purdue University  
West Lafayette, IN 47907, USA  
E-mail: omalis@purdue.edu

B. Dzuba, A. Senichev, R. E. Diaz, M. J. Manfra  
Birck Nanotechnology Center  
Purdue University  
West Lafayette, IN 47907, USA

 The ORCID identification number(s) for the author(s) of this article can be found under <https://doi.org/10.1002/pssb.202100569>.

© 2022 The Authors. physica status solidi (b) basic solid state physics published by Wiley-VCH GmbH. This is an open access article under the terms of the Creative Commons Attribution-NonCommercial-NoDerivs License, which permits use and distribution in any medium, provided the original work is properly cited, the use is non-commercial and no modifications or adaptations are made.

DOI: 10.1002/pssb.202100569

B. A. Magill, G. A. Khodaparast  
Department of Physics  
Virginia Tech  
Blacksburg, VA 24061, USA

A. Senichev, M. J. Manfra  
Elmore Family School of Electrical and Computer Engineering  
Purdue University  
West Lafayette, IN 47907, USA

M. J. Manfra  
School of Materials Engineering  
Purdue University  
West Lafayette, IN 47907, USA

S. McGill, C. Garcia  
National High Magnetic Field Laboratory  
Tallahassee, FL 32310, USA

C. Garcia  
Department of Physics  
Florida State University  
Tallahassee, FL 32306, USA

the design of green light-emitting diodes (LEDs) with high IQE.<sup>[8,13]</sup> Nonpolar structures based on III-nitride materials have also shown potential for infrared devices.<sup>[14,15]</sup> This article presents a study of continuous-excitation and time-resolved photoluminescence (TRPL) of nonpolar m-plane InGaN/AlGaIn multi-QWs designed for infrared applications.

The properties of III-nitrides are strongly affected by strain. The high density of defects produced by strain buildup can introduce significant nonradiative recombination.<sup>[8,16,17]</sup> Furthermore, strain is anisotropic on the m-plane and generates significant alloy inhomogeneity and interface roughness in m-plane AlGaIn/GaN QWs with Al compositions above 50%.<sup>[18]</sup> Therefore, to mitigate strain-induced issues, this study focuses on nearly strain-balanced m-plane InGaIn/AlGaIn heterostructures.<sup>[19,20]</sup>

Carrier localization and recombination play important roles in determining III-nitride device performance. The electron–hole recombination lifetime is essential for visible III-nitride LEDs.<sup>[21]</sup> Carrier localization may enhance visible light emission by preventing carriers from being trapped by defect-related nonradiative recombination centers.<sup>[22]</sup> Depending on the character of the localization sites,<sup>[21]</sup> charge localization can also impact recombination lifetime. Moreover, localization potentials can reduce the degree of polarization of the emitted light,<sup>[23]</sup> and contribute to accelerated device aging.<sup>[24]</sup> Since charge localization originates from band-structure fluctuations, it affects the linewidth of both interband and intersubband emission. Therefore, investigating carrier localization and recombination provides unique insights into the band structure and carrier dynamics of all optoelectronic devices.

While extensive studies of recombination and localization have been performed for polar c-plane InGaIn/(Al)GaIn QWs, considerably fewer studies have been reported for nonpolar m-plane QWs. Furthermore, most of the optical studies on nonpolar m-plane structures published to date are limited to samples grown by metal–organic chemical vapor deposition (MOCVD).<sup>[8,21–32]</sup> This article presents an original study of carrier recombination and localization in nearly strain-balanced nonpolar multi-QWs grown by plasma-assisted molecular beam epitaxy (PAMBE). PAMBE is of particular interest because it achieves growth of In-containing nonpolar III-nitrides at a significantly lower temperature than MOCVD, and consequently produces materials with distinct structures at the nanoscale. Moreover, the low growth temperature of PAMBE may enable InGaIn with a lower point defect density for longer wavelength emission.<sup>[30,33]</sup>

## 2. Experimental and Calculation Details

The PL measurements were performed on m-plane superlattices consisting of 15 In<sub>0.09</sub>Ga<sub>0.91</sub>N QWs with Al<sub>0.19</sub>Ga<sub>0.81</sub>N barriers grown by PAMBE. The details of the growth process are given elsewhere.<sup>[20]</sup> Briefly, the PAMBE system was equipped with conventional effusion cells for indium, gallium, aluminum, and silicon. The active nitrogen flux was supplied by a Veeco Unibulb radio-frequency plasma source operated at 300 W forward power with 0.5 sccm of nitrogen (N<sub>2</sub>) flow. The superlattices were grown at 565 °C on commercially available nonpolar m-plane (10 $\bar{1}0$ ) semi-insulating GaN substrates from

Nanowin, Inc. The 5 × 10 mm<sup>2</sup> substrates were miscut –0.5° ± 0.2° toward the c-axis, had a surface root mean square roughness of less than 0.3 nm over 16 μm<sup>2</sup>, and nominal threading dislocation density of less than 5 × 10<sup>6</sup> cm<sup>–2</sup>.

The well and barrier thicknesses were chosen to minimize strain accumulation while keeping the Al composition in the barriers low enough to avoid aluminum segregation. We used the thickness-weighted method to approximate strain-balanced conditions:  $\epsilon_b t_b + \epsilon_w t_w = 0$ , where  $\epsilon_b$  and  $\epsilon_w$  represent the strain in the barrier and well, respectively, while  $t_b$  and  $t_w$  represent their respective layer thicknesses. Note that strain is anisotropic on the m-plane surface, and thus cannot be exactly balanced along both the a-axis and c-axis simultaneously. Therefore, we selected the barrier thickness (6.4 nm) and QW thickness (3 nm) so that strain was roughly balanced along the a-direction and there is less than 0.3% residual strain per period along the c-direction. The samples are either undoped (Sample G) or  $\delta$ -doped (Sample H) in the barriers with two sheets of silicon located  $\approx 1$  nm away from each barrier/QW interface.<sup>[19]</sup> The density of dopant is about 2 × 10<sup>14</sup> cm<sup>–2</sup>, which results in a calculated electron density of 8.6 × 10<sup>12</sup> cm<sup>–2</sup> in each QW.

The samples were characterized with high-resolution X-ray diffraction (HRXRD).<sup>[20]</sup>  $\omega$ -2 $\theta$  spectra were collected by a PANalytical X'Pert-MRD high-resolution X-ray diffractometer equipped with a 4-bounce Ge monochromator. To extract layer thicknesses and alloy compositions, the software package Epitaxy 4.5a from PANalytical was used to simulate the HRXRD diffraction patterns.

The continuous-excitation PL experiments were performed using a 325 nm cw He–Cd laser. The excitation power was about 10 mW with an estimated excitation carrier density of 6.3 × 10<sup>11</sup> cm<sup>–3</sup>. This is weak excitation which does not significantly affect the band structure.<sup>[34,35]</sup> The samples were placed in a liquid helium flow cryostat and measured in reflection geometry in the range from 8 K to room temperature. The PL spectra were collected by a Cary Eclipse Fluorescence Spectrometer equipped with a photomultiplier tube. The spectra were corrected by subtracting a linear background and fitting with a Gaussian function to extract the transition energy and full-width-at-half-maximum (FWHM).

Time-resolved photoluminescence (TRPL) was measured in a helium flow-through cryostat from 2 to 100 K temperature range. In our measurements, we used femtosecond 784 nm pulses which were upconverted to 384 nm, using a nonlinear crystal (BBO) generating an average power of  $\approx 80$   $\mu$ W (photoinduced density  $\approx 4.8 \times 10^{14}$  cm<sup>–3</sup>). The pulses were from a Mira 900 Ti:sapphire oscillator with a repetition rate of 80 MHz. Light emitted at the PL peak ( $\approx 408$  nm) was selected using a monochromator then collected from the sample in a reflectivity geometry, using an avalanche photodiode. A Faraday geometry was used in magnetic field dependence TRPL measurements, where the direction of the field is perpendicular to the epilayer plane. A time-correlated single-photon counting system (PicoHarp 300) was used to determine the time between the excitation pulse and emission of PL photons.

The Nextnano software package for self-consistent simulation of the band structures of our InGaIn/AlGaIn superlattices was used.<sup>[36]</sup> Free electrons and holes are likely to form excitons and then recombine to emit photons, so the calculated PL

energies were corrected to include the exciton binding energy. The energy shift due to this effect was expected to be less than 60 meV.<sup>[27]</sup> The simple hydrogen atom-like model was used to estimate the energy shift, where the excitonic binding energy was calculated using

$$E_x = \frac{m_r R_y(H)}{m_0 \epsilon^2} \quad (1)$$

where  $m_0$  is the free-electron mass, and  $m_r$  is the reduced mass of the effective masses of electron and hole in the exciton.  $R_y(H) \approx 13.6\text{eV}$  is the Rydberg energy.  $m_r \approx 0.17m_0$ ,<sup>[37,38]</sup> and  $\epsilon \approx 10$ .<sup>[27]</sup>

### 3. Results and Discussion

We previously found that the experimental PL energies of m-plane InGaN/AlGaIn superlattices are systematically lower than the calculations made using generally accepted material parameters.<sup>[19]</sup> At 8 K, the experimental PL peaks are 3.095 eV (sample G) and 3.079 eV (sample H), while the calculated PL energies are 3.299 eV (sample G) and 3.302 eV (sample H). The discrepancy was attributed to the inhomogeneous distribution of In composition,<sup>[19]</sup> but may also be due to other excitonic effects that were not included in the calculation.<sup>[39]</sup> We note that at 80 K, the average PL degree of polarization for both samples is about 81%, which agrees with previous reports.<sup>[22]</sup>

It is generally accepted that the PL signal at low temperature is due to the recombination of localized excitons. We have already reported the “S-shape” dependence of the PL peak position as a function of temperature that is typically associated with exciton localization.<sup>[19]</sup> Exciton localization in nonpolar InGaN/GaN QWs was attributed to strong hole localization at indium-rich fluctuations in the quantum wells.<sup>[8]</sup> In the absence of intrinsic and piezoelectric fields on the m-plane, the electrons are no longer localized by well-width fluctuations, and are only bound by Coulomb interaction to the localized holes.<sup>[8]</sup> In our case of m-plane InGaN/AlGaIn QWs, there is no evidence for quantum dot-like structures.<sup>[19]</sup> Considering the size and indium composition of our QWs, the localized states also cannot originate from nanoscopic sites with relaxed strain.<sup>[33]</sup> Therefore, it is likely that in our nearly strain-balanced superlattices, indium-rich regions are the main source of localization centers.<sup>[22,40]</sup>

Carrier localization is reflected in the linewidth of the PL spectrum and its temperature dependence. **Figure 1** shows the temperature dependence of the FWHM of the continuous excitation PL for samples G<sup>[19]</sup> and H. The linewidth is the result of homogeneous and inhomogeneous broadening. The homogeneous broadening comes from the scattering of the excitons by acoustic phonons, which have a linear temperature dependence, and the interaction of the excitons with longitudinal–optical (LO) phonons, which is proportional to Bose–Einstein distribution.<sup>[41]</sup> Thus, the total broadening has a temperature dependence following the relationship

$$\Gamma(T) = \alpha \left( e^{\frac{E_{LO}}{k_B T}} - 1 \right)^{-1} + \Gamma_{ih} + \beta T \quad (2)$$

where  $E_{LO}$  represents the LO phonon energy,  $E_{LO} = 90\text{meV}$ ,<sup>[42]</sup>  $\alpha$  and  $\beta$  are the coupling strengths of the interaction of excitons

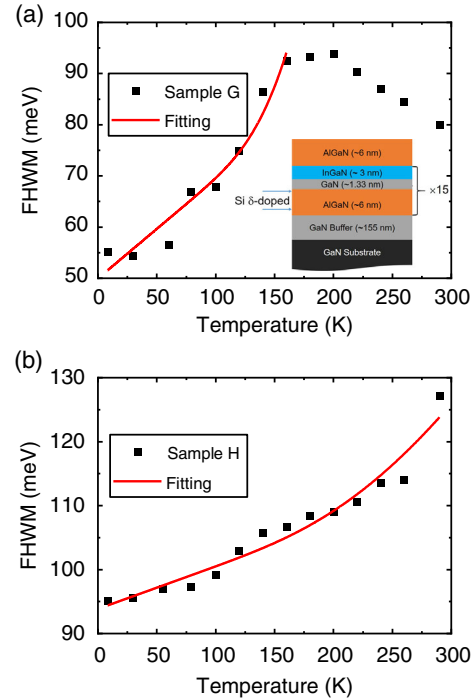


**Figure 1.** Temperature dependence of PL FWHM for: a) undoped sample G,<sup>[19]</sup> and b) doped sample H. The data in panel (a) was reproduced from Ref. [19] with permission of AIP Publishing. Red lines are fits based on the temperature dependence of total broadening (Equation (2)).

with LO and acoustic phonons, respectively.  $\Gamma_{ih}$  denotes inhomogeneous broadening. By fitting the temperature dependence of the FWHM with Equation (2) at low temperatures (Figure 1), we obtain inhomogeneous broadenings of  $51 \pm 3\text{meV}$  (sample G) and  $94 \pm 2\text{meV}$  (sample H) ( $\alpha = 9603.55\text{meV}$ ,  $\beta = 0.19392\text{meV K}^{-1}$  for sample G, and  $\alpha = 397.45\text{meV}$ ,  $\beta = 0.06646\text{meV K}^{-1}$  for sample H). We emphasize that these values characterize only the low-temperature state. In general, inhomogeneous broadening depends on the distribution of thermalized charges and therefore on temperature.

To evaluate the exciton localization depth, we assume the localization centers have a Gaussian distribution.<sup>[43,44]</sup> The PL intensity under weak excitation is then given by<sup>[44]</sup>

$$I_{PL}(E) \propto \int_{-\infty}^{+\infty} (2\pi\sigma^2)^{-\frac{1}{2}} e^{-\frac{E-E_1}{2\sigma^2}} g_0(E-E_1) dE_1 \quad (3)$$

where  $\sigma$  is the localization depth parameter, and  $g_0(E)$  is the density of states for an ideal QW. Since  $\Gamma_{ih} \approx 2.35\sigma$ , we can estimate the localization depth from the inhomogeneous broadening.

The average localization depth for the undoped sample G is estimated to be  $21 \pm 1\text{meV}$ . This depth is smaller than previously reported values for m-plane InGaN/(Al)GaIn QWs. For example, Liuolia et al. reported an average localization depth of 46 meV for a nonpolar m-plane 2.5 nm InGaIn QW.<sup>[44]</sup> C-plane QWs were found to have even larger average localization depths, as large as 80 meV.<sup>[45]</sup> The small localization depth of our undoped heterostructures is a direct consequence of our PL lines being narrower than previously reported in the literature for the

m-plane InGaN/GaN QWs,<sup>[8,22,46,47]</sup> and is likely due to very different growth conditions employed by PAMBE as compared to previous reports that employed MOCVD.

The doped sample H has a much larger inhomogeneous broadening ( $94 \pm 2$  meV), which corresponds to an average localization depth of approximately  $40 \pm 1$  meV. Deposition of silicon in the barriers directly enhances the potential fluctuations experienced by excitons by affecting the alloy uniformity in the QWs and barriers, and increasing interface roughness. Impurity scattering may also contribute to the additional inhomogeneous broadening in the doped samples.

TRPL measurements in the temperature range 2–100 K identified two decay time scales for sample G.<sup>[19]</sup> The inset of **Figure 2** shows the TRPL for samples G and H at 100 K. At 2 K, the fast decay time  $\tau_1$  is  $0.330 \pm 0.002$  ns, while the slow decay time  $\tau_2$  is  $2.18 \pm 0.06$  ns, approximately 7 times longer than the initial fast decay time. The origin of these two time decays is not completely understood at this point, but we attribute them to two different types of localization centers (referred to as A and B henceforth). We note that dual localization centers have been previously reported in m-plane InGaN/GaN QWs.<sup>[44]</sup> In contrast, sample H shows only one decay constant, which indicates a single type of localization center (referred to as C). At 2 K, this decay time,  $\tau$ , of  $0.283 \pm 0.002$  ns, is slightly lower than  $\tau_1$ . All three decay times are much shorter than those in polar c-plane structures, in agreement with the expectation that recombination is much faster in nonpolar m-plane structures.<sup>[21,48,49]</sup> As temperature increases, bound excitons start to dissociate at  $\approx 100$  K. The generated free excitons contribute to the increase of FWHM.<sup>[22]</sup> In sample G, excitons will redistribute between the two types of localization centers, resulting in a non-monotonic temperature dependence of FWHM above 100 K (Figure 1a).

Samples G and H were designed to have the same nominal layer structure and to differ only in the doping profile. The additional doping of sample H is not expected to significantly perturb the electronic band structure, and therefore, the calculated PL peak energies are very close to each other ( $\approx 3.3$  eV). The agreement between the measured PL energies of the two samples

confirms that they have the intended identical layer structures. Moreover, the decay times,  $\tau_1$  and  $\tau$ , of localization centers, A and C are quantitatively similar, and have analogous temperature<sup>[19]</sup> and magnetic field dependence curves (see the following discussion). In contrast, the decay time  $\tau_2$  of localization center B is much longer. As temperature increases, all of the three decay times decrease, but the changes of  $\tau_1$  and  $\tau$  are less dramatic than that of  $\tau_2$ . Over the measured temperature range (2–100 K), both  $\tau_1$  and  $\tau$  decrease about 22%, while  $\tau_2$  decreases about 38%.<sup>[19]</sup> Therefore, we believe the sub-nanosecond decay processes A and C are due to the same type of localization centers that likely originate from indium-rich regions in the QWs.

The nanosecond decay time  $\tau_2$  clearly has a different origin than the sub-nanosecond decay times  $\tau_1$  and  $\tau$ . In m-plane InGaN/GaN QWs, long decay times in the range of several to tens of nanoseconds have also been reported,<sup>[23,50,51]</sup> and have been attributed to localized states or to nonradiative recombination of extended states.<sup>[23]</sup> Since theoretical modeling<sup>[27]</sup> has shown that an electron charge density may spread in-plane over a region with a diameter as large as 5 nm, center B is possibly due to alloy fluctuations in the AlGaIn barriers that localize the electron and hole distributions at different in-plane sites. As the temperature increases,  $\tau_2$  decreases faster than the other two decay times due to nonradiative recombination in the barriers.<sup>[19]</sup>

The total PL decay time  $\tau_{\text{PL}}$  is related to the radiative recombination lifetime  $\tau_r$  and nonradiative recombination lifetime  $\tau_{\text{nr}}$  by the relation

$$\frac{1}{\tau_{\text{PL}}} = \frac{1}{\tau_r} + \frac{1}{\tau_{\text{nr}}} \quad (4)$$

The peak intensity of TRPL transients is approximately proportional to the radiative recombination rate.<sup>[21,52,53]</sup> At a temperature lower than 5 K, major nonradiative recombination centers, such as the Shockley–Read–Hall (SRH) recombination centers are not significantly activated.<sup>[48]</sup> Therefore, the decay times we obtained at 2 K are dominated by radiative recombination. As temperature increases, the maximum transient PL intensity decreases as shown in Figure 2. This decrease may be due to an increase in radiative recombination lifetime. However, since the total PL decay time also decreases with temperature, it is more likely that the nonradiative recombination lifetime decreases, indicating that localized excitons are thermally activated to extended states and then get captured by nonradiative recombination centers.

We fit the temperature dependence of  $\tau_1$  with the model proposed by Shahmohammadi et al.<sup>[54,55]</sup> assuming the radiative decay of localized excitons is temperature activated with an activation energy  $E_{\text{loc}} = 21$  meV, estimated from our continuous PL measurements, and a time constant,  $\tau_{\text{loc}}$ , equal to the measured value at 2 K (0.33 ns). The free exciton lifetime is assumed to increase linearly with temperature.<sup>[54]</sup> The nonradiative decay is also modeled as a temperature-activated process with an activation energy of  $E_A = 200$  meV, and high-temperature time constant  $\tau_{\text{nr},0} = 100$  ps.<sup>[54]</sup> The experimental data is reproduced by a localization center density,  $N_D$ , of approximately  $6 \times 10^{12} \text{ cm}^{-2}$ , in agreement with previous reports.<sup>[54]</sup>

In sample H, the doping electrons occupy all localized and some extended electronic states and allow recombination of all

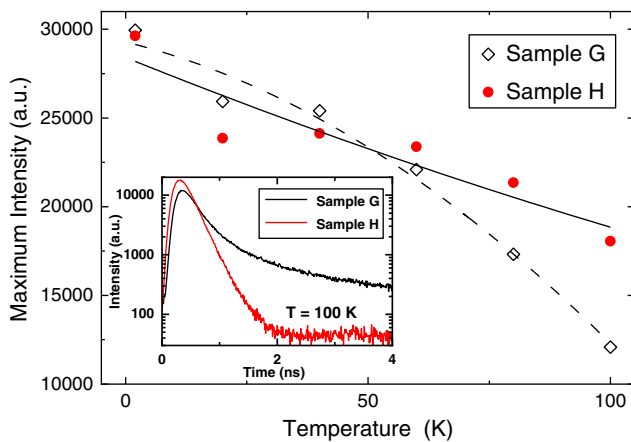


**Figure 2.** Temperature dependence of transient PL peak intensity for the undoped sample G and the doped sample H. The lines are guides to the eye. The inset shows the TRPL for the two samples at 100 K.



holes via the fast decay path. Therefore, sample H does not exhibit the second decay path, characterized as  $\tau_2$  in sample G. Also, the transient PL peak intensity of sample H decreases slower with increasing temperature than the transient peak of sample G (Figure 2) because thermally activated electrons that may be trapped by nonradiative recombination centers in the barriers have a smaller contribution to transient PL intensity.

TRPL in the magnetic field was performed to evaluate the degree of exciton localization at 2 K (Figure 3). The addition of a magnetic field enhances the localization of excitons.<sup>[56]</sup> With an increasing magnetic field, we observed an increase of transient PL peak intensity for sample G (inset of Figure 3a). We attribute this increase of radiative recombination rate (and associated radiative decay lifetime decrease) to an increased overlap of the electron and hole wavefunctions. Sample H exhibits the opposite trend. The transient PL peak intensity decreases with increasing magnetic field (inset of Figure 3b). The increased localization in sample H probably enhances nonradiative recombination associated with the additional doping. This enhanced nonradiative recombination may be due to additional structural defects and/or to Auger recombination.

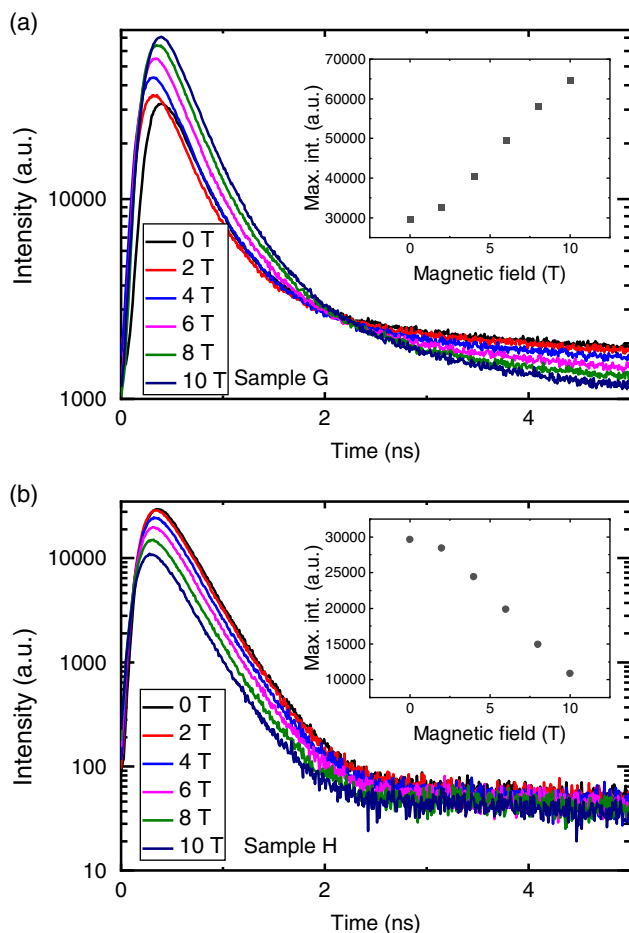


**Figure 3.** a) TRPL for undoped sample G and b) doped sample H in magnetic fields. The insets show the dependence of the TRPL maximum on the magnetic field for each sample.

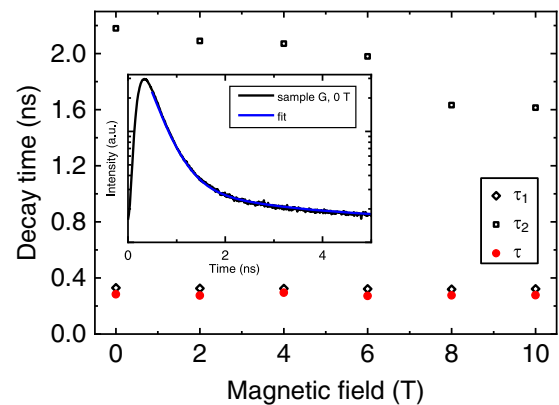


**Figure 4.** Magnetic field dependence of decay times  $\tau_1$  and  $\tau_2$  for sample G, and  $\tau$  for sample H at 2 K. The inset shows the fit of the TRPL for sample G with two exponential decays at zero magnetic field.

The magnetic field dependence of the decay times for samples G and H is shown in Figure 4. The inset of Figure 4 shows an example of the fitting of the TRPL with exponential decays at 2 K and zero magnetic field. As the magnetic field increases from 0 to 10 T,  $\tau_1$  and  $\tau$  decrease only slightly (2%), while  $\tau_2$  decreases significantly (26%). We conclude that the localization of excitons in centers A and C is not appreciably affected by the magnetic field. For localization center B, however, not only all excitons are in the ground state, but also occupy the extended state. Therefore, the increased magnetic field enhances the localization effect, and  $\tau_2$  decreases as a result of a decrease in the radiative recombination lifetime.

## 4. Conclusion

Temperature-dependent continuous-excitation and TRPL measurements were performed on nearly strain-balanced m-plane  $\text{In}_x\text{Ga}_{1-x}\text{N}/\text{Al}_y\text{Ga}_{1-y}\text{N}$  ( $x = 0.09$ ,  $y = 0.19$ ) multi-QWs grown by PAMBE. Dual localization centers were identified in undoped structures, while only a single type of localization center was found in doped structures. The localization centers characterized by sub-nanosecond time constants are likely due to indium fluctuations in the QWs, while those characterized by a nanosecond decay time are likely due to alloy inhomogeneity in the barriers. We attribute the absence of the second decay pathway in doped samples to the effect of the doping sheets. The average localization depth of 21 meV was extracted from continuous-excitation PL measurements in undoped samples. This depth is much smaller than that reported in polar structures or in previously reported m-plane  $\text{InGaN}/\text{GaN}$  QWs grown by MOCVD. Temperature-dependent TRPL allowed us to estimate the density of localization centers in undoped samples as  $6 \times 10^{12} \text{ cm}^{-2}$ . Furthermore, TRPL indicates that at the lowest temperatures, carrier localization in the QWs is insensitive to the magnetic field. In contrast, the decay time of excitons localized by barrier fluctuations decreases with an increasing magnetic field.

## Acknowledgements

The authors acknowledge support from the National Science Foundation. Y. C., T. N., and O. M. acknowledge partial support from NSF award DMR-1610893, and DMR-2004462. A. S. and B. D. were supported from NSF award ECCS-1607173. G. A. K. and B. A. M. acknowledge the support from AFOSR under Grant FA9550-17-1-0341. A portion of this work was performed at the National High Magnetic Field Laboratory, which is supported by the National Science Foundation Cooperative Agreement No. DMR-1644779 and the State of Florida.

## Conflict of Interest

The authors declare no conflict of interest.

## Data Availability Statement

The data that support the findings of this study are available from the corresponding author upon reasonable request.

## Keywords

localization, nitrides, photoluminescence, recombination

Received: November 5, 2021

Revised: February 7, 2022

Published online:

- [1] T. D. Moustakas, P. Paiella, *Rep. Prog. Phys.* **2017**, *80*, 106501.
- [2] Q. Dai, M. F. Schubert, J. K. Kim, D. D. Koleske, M. H. Crawford, S. R. Lee, A. J. Fischer, G. Thaler, M. A. Banas, *Appl. Phys. Lett.* **2009**, *94*, 111109.
- [3] A. Hangleiter, D. Fuhrmann, M. Grewe, F. Hitzel, G. Klewer, S. Lahmann, C. Netzel, N. Riedel, U. Rossow, *Phys. Status Solidi A* **2004**, *201*, 2808.
- [4] Y. L. Li, Y. R. Huang, Y. H. Lai, *Appl. Phys. Lett.* **2007**, *91*, 181113.
- [5] T. Takeuchi, S. Sota, M. Katsuragawa, M. Komori, H. Takeuchi, H. Amano, I. Akasaki, *Jpn. J. Appl. Phys.* **1997**, *36*, L382.
- [6] F. Bernardini, V. Fiorentini, D. Vanderbilt, *Phys. Rev. B* **2001**, *63*, 193201
- [7] O. Mayrock, H.-J. Wunsche, F. Henneberger, *Phys. Rev. B* **2000**, *62*, 16870.
- [8] P. Dawson, S. Schulz, R. A. Oliver, M. J. Kappers, C. J. Humphreys, *J. Appl. Phys.* **2016**, *119*, 181505.
- [9] O. Malis, C. Edmunds, M. J. Manfra D. L. Sivco, *Appl. Phys. Lett.* **2009**, *94*, 161111.
- [10] C. Edmunds, L. Tang, D. Li, M. Cervantes, G. Gardner, T. Paskova, M. J. Manfra, O. Malis, *J. Electron. Mater.* **2012**, *41*, 881.
- [11] C. Edmunds, L. Tang, J. Shao, D. Li, M. Cervantes, G. Gardner, D. N. Zakharov, M. J. Manfra, O. Malis, *Appl. Phys. Lett.* **2012**, *101*, 102104.
- [12] C. Edmunds, L. Tang, M. Cervantes, M. Shirazi-HD, J. Shao, A. Grier, A. Valavanis, J. D. Cooper, D. Li, G. Gardner, D. N. Zakharov, Z. Ikonc, D. Indjin, P. Harrison, M. J. Manfra, O. Malis, *Phys. Rev. B* **2013**, *88*, 235306.
- [13] S.-C. Ling, T.-C. Lu, S.-P. Chang, J.-R. Chen, H.-C. Kuo, S.-C. Wang, *Appl. Phys. Lett.* **2010**, *96*, 231101.
- [14] C. Edmunds, J. Shao, M. Shirazi-HD, M. Manfra, O. Malis, *Appl. Phys. Lett.* **2014**, *105*, 021109.
- [15] D. Feezell, Y. Sharma, S. Krishna, *J. Appl. Phys.* **2013**, *113*, 1133103.
- [16] S. Saito, R. Hashimoto, J. Hwang, S. Nunoue, *Appl. Phys. Express* **2013**, *6*, 111004.
- [17] T. B. Eldred, M. Abdelhamid, J. G. Reynolds, N. A. El-Masry, J. M. LeBeau, S. M. Bedair, *Appl. Phys. Lett.* **2020**, *116*, 102104.
- [18] M. Shirazi-HD, R. E. Diaz, T. Nguyen, J. Jian, G. C. Gardner, H. Wang, M. J. Manfra, O. Malis, *J. Appl. Phys.* **2018**, *123*, 161581.
- [19] Y. Cao, B. Dzuba, B. Magill, A. Senichev, T. Nguyen, R. Diaz, M. Manfra, S. McGill, C. Garcia, G. Khodaparast, O. Malis, *J. Appl. Phys.* **2020**, *127*, 185702.
- [20] B. Dzuba, A. Senichev, T. Nguyen, Y. Cao, R. E. Diaz, M. J. Manfra, O. Malis, *J. Appl. Phys.* **2020**, *128*, 115701.
- [21] S. Marcinkevičius, K. M. Kelchner, L. Y. Kuritzky, S. Nakamura, S. P. DenBaars, J. S. Speck, *Appl. Phys. Lett.* **2013**, *103*, 111107.
- [22] S. Marcinkevičius, K. M. Kelchner, S. Nakamura, S. P. DenBaars, J. S. Speck, *Appl. Phys. Lett.* **2013**, *102*, 101102.
- [23] V. Liuolia, S. Marcinkevičius, Y.-D. Lin, H. Ohta, S. P. DenBaars, S. Nakamura, *J. Appl. Phys.* **2010**, *108*, 023101.
- [24] A. Pinos, S. Marcinkevičius, J. Yang, Y. Bilenko, M. Shatalov, R. Gaska, M. S. Shur, *Appl. Phys. Lett.* **2009**, *95*, 181914.
- [25] D. Sutherland, T. Zhu, J. T. Griths, F. Tang, P. Dawson, D. Kundys, F. Oehler, M. J. Kappers, C. J. Humphreys, R. A. Oliver, *Phys. Status Solidi B* **2015**, *252*, 965.
- [26] D. Kundys, D. Sutherland, M. J. Davies, F. Oehler, J. Griths, P. Dawson, M. J. Kappers, C. J. Humphreys, S. Schulz, F. Tang, R. A. Oliver, *Sci. Technol. Adv. Mater.* **2016**, *17*, 736.
- [27] S. Schulz, D. P. Tanner, E. P. O'Reilly, M. A. Caro, T. L. Martin, P. A. J. Bagot, M. P. Moody, F. Tang, J. T. Griths, F. Oehler, M. J. Kappers, R. A. Oliver, C. J. Humphreys, D. Sutherland, M. J. Davies, P. Dawson, *Phys. Rev. B* **2015**, *92*, 235419.
- [28] S. Marcinkevičius, K. M. Kelchner, S. Nakamura, S. P. DenBaars, J. S. Speck, *Phys. Status Solidi C* **2014**, *11*, 690.
- [29] K. M. Kelchner, L. Y. Kuritzky, K. Fujito, S. Nakamura, S. P. DenBaars, J. S. Speck, *J. Cryst. Growth* **2013**, *382*, 80.
- [30] M. Sawicka, P. Wolny, M. Kryko, H. Turski, K. Szkudlarek, S. Grzanka, C. Skierbiszewski, *J. Cryst. Growth* **2017**, *465*, 43.
- [31] S. Kusanagi, Y. Kanitani, Y. Kudo, K. Tasai, A. A. Yamaguchi, S. Toriya, *Jpn. J. Appl. Phys.* **2019**, *58*, SCCB28.
- [32] A. Pesach, E. Gross, C.-Y. Huang, Y.-D. Lin, S. E. Schacham, S. Nakamura, G. Bahir, *Appl. Phys. Lett.* **2013**, *103*, 022110.
- [33] A. Senichev, T. Nguyen, R. E. Diaz, B. Dzuba, M. Shirazi-HD, Y. Cao, M. J. Manfra, O. Malis, *APL Mater.* **2019**, *7*, 121109.
- [34] M. Funato, Y. Kawakami, *J. Appl. Phys.* **2008**, *103*, 093501.
- [35] A. Kaneta, M. Funato, Y. Kawakami, *Phys. Rev. B* **2008**, *78*, 125317.
- [36] S. Birner, T. Zibold, T. Andlauer, T. Kubis, M. Sabathil, A. Trellakis, P. Vogl, *IEEE Trans. Electron Devices* **2007**, *54*, 2137.
- [37] I. Vurgaftman, J. R. Meyer, *J. Appl. Phys.* **2003**, *94*, 3675.
- [38] Ursula M. E. Christmas, A. D. Andreev, D. A. Faux, *J. Appl. Phys.* **2005**, *98*, 073522.
- [39] I. Pelant, J. Valenta, *Luminescence Spectroscopy of Semiconductors*, Oxford University Press, New York **2016**.
- [40] C. H. Chiu, S. Y. Kuo, M. H. Lo, C. C. Ke, T. C. Wang, Y. T. Lee, H. C. Kuo, T. C. Lu, S. C. Wang, *J. Appl. Phys.* **2009**, *105*, 063105.
- [41] S. J. Xu, L. X. Zheng, S. H. Cheung, M. H. Xie, S. Y. Tong, H. Yang, *Appl. Phys. Lett.* **2002**, *81*, 4389.
- [42] M. Beeler, E. Trichas, E. Monroy, *Semicond. Sci. Technol.* **2013**, *28*, 074022.
- [43] P. G. Eliseev, P. Perlin, J. Lee, M. Osinski, *Appl. Phys. Lett.* **1997**, *71*, 569.
- [44] V. Liuolia, A. Pinos, S. Marcinkevičius, Y. D. Lin, H. Ohta, S. P. DenBaars, S. Nakamura, *Appl. Phys. Lett.* **2010**, *97*, 151106.

- [45] V. Liuolia, S. Marcinkevičius, A. Pinos, R. Gaska, M. S. Shur, *Appl. Phys. Lett.* **2009**, *95*, 091910.
- [46] C. Mounir, U. T. Schwarz, I. L. Koslow, M. Kneissl, T. Wernicke, *Phys. Rev. B* **2016**, *93*, 235314.
- [47] R. Ivanov, S. Marcinkevičius, M. D. Mensi, O. Martinez, L. Y. Kuritzky, D. J. Myers, S. Nakamura, J. S. Speck, *Phys. Rev. Appl.* **2017**, *7*, 064033.
- [48] Y. Xing, L. Wang, D. Yang, Z. Wang, Z. Hao, C. Sun, B. Xiong, Y. Luo, Y. Han, J. Wang, H. Li, *Sci. Rep.* **2017**, *7*, 45082.
- [49] M. Pophristic, F. H. Long, C. Tran, I. T. Ferguson, R. F. Karlicek Jr., *J. Appl. Phys.* **1999**, *86*, 1114.
- [50] G. A. Garrett, H. Shen, M. Wraback, A. Tyagi, M. C. Schmidt, J. S. Speck, S. P. DenBaars, S. Nakamura, *Phys. Status Solidi C* **2009**, *6*, S800.
- [51] Y. Huang, K. W. Sun, A. M. Fischer, Q. Y. Wei, R. Juday, F. A. Ponce, R. Kato, T. Yokogawa, *Appl. Phys. Lett.* **2011**, *98*, 261914.
- [52] E. Berkowicz, D. Gershoni, G. Bahir, E. Lakin, D. Shilo, E. Zolotoyabko, A. C. Abare, S. P. DenBaars, L. A. Coldren, *Phys. Rev. B* **2000**, *61*, 10994.
- [53] O. Brandt, H. Yang, K. H. Ploog, *Phys. Rev. B* **1996**, *54*, R5215.
- [54] M. Shahmohammadi, W. Liu, G. Rossbach, L. Lahourcade, A. Dussaigne, C. Bougerol, R. Butté, N. Grandjean, B. Deveaud, G. Jacopin, *Phys. Rev. B* **2017**, *95*, 125314.
- [55] P. Corfdir, J. Levrat, A. Dussaigne, P. Lefebvre, H. Teisseyre, I. Grzegory, T. Suski, J.-D. Ganière, N. Grandjean, B. Deveaud-Plédran, *Phys. Rev. B* **2011**, *83*, 245326.
- [56] T. R. Merritt, M. A. Meeker, B. A. Magill, G. A. Khodaparast, S. McGill, J. G. Tischler, S. G. Choi, C. J. Palmstrøm, *J. Appl. Phys.* **2014**, *115*, 193503.